Original research

Impedance-based sensors discriminate among different types of blood thrombi with very high specificity and sensitivity

Pierluca Messina ![ORCID],[1] Cédric Garcia,[2,3,4] Joachim Rambeau,[1] Jean Darcourt,[2,3,5] Ronan Balland,[1] Bruno Carreel,[1] Myline Cottance,[1] Elena Gusarova,[1] Julie Lafaurie-Janvore,[1] Gor Lebedev,[1] Franz Bozsak,[1] Abdul I Barakat,[6] Bernard Payrastre,[2,3,4] Christophe Cognard[2,3,5]

ABSTRACT

Background Intracranial occlusion recanalization fails in 20% of endovascular thrombectomy procedures, and thrombus composition is likely to be an important factor. In this study, we demonstrate that the combination of electrical impedance spectroscopy (EIS) and machine learning constitutes a novel and highly accurate method for the identification of different human thrombus types.

Methods 134 samples, subdivided into four categories, were analyzed by EIS: 29 'White', 26 'Mixed', 12 'Red' thrombi, and 67 liquid 'Blood' samples. Thrombi were generated in vitro using citrated human blood from five healthy volunteers. Histological analysis was performed to validate the thrombus categorization based on red blood cell content. A machine learning prediction model was trained on impedance data to differentiate blood samples from any type of thrombus and in between the four sample categories.

Results Histological analysis confirmed the similarity between the composition of in vitro generated thrombi and retrieved human thrombi. The prediction model yielded a sensitivity/specificity of 90%/99% for distinguishing blood samples from thrombi and a global accuracy of 88% for differentiating among the four sample categories.

Conclusions Combining EIS measurements with machine learning provides a highly effective approach for discriminating among different thrombus types and liquid blood. These findings raise the possibility of developing a probe-like device (eg, a neurovascular guidewire) integrating an impedance-based sensor. This sensor, placed in the distal part of the smart device, would allow the characterization of the probed thrombus on contact. The information could help physicians identify optimal thrombectomy strategies to improve outcomes for stroke patients.

INTRODUCTION

In recent years, endovascular thrombectomy (EVT) has emerged as the most effective treatment for large-vessel ischemic stroke, a particularly life-threatening and debilitating form of stroke.[1] Despite significant advances, three quarters of procedures require two or more retrieval attempts, and 20% of EVT procedures fail.[2,3] While the precise reasons for EVT failure remain poorly understood, there is mounting evidence that thrombus composition is a key factor influencing repeat thrombectomy maneuvers and consequent treatment failure.[3–13] Recent clinical and in vitro data suggest that fibrin/platelet-rich thrombi are more resistant to thrombectomy and lead to poorer revascularization outcomes,[3,9] while red blood cell (RBC)-rich thrombi are associated with a reduced number of recanalization maneuvers which in turn yields better clinical outcomes.[14–18] Hence, identifying the composition of the thrombus causing the stroke promises to provide critical insight into the most effective treatment approaches for avoiding repeat revascularization maneuvers and treatment failure. Using MRI or CT for discriminating between RBC-rich and fibrin/platelet-rich thrombi has met with limited success.[9,19–22] These preoperative imaging modalities are thus not used in the decision-making process and cannot provide real time characterization of the thrombus during EVT. Alternative techniques for the discrimination of different thrombus types are highly desirable. We hypothesized that electrochemical impedance spectroscopy (EIS) may provide such a technique.[23]

EIS constitutes a robust and real-time technique for characterizing biological tissues. By placing a pair of electrodes in contact with the tissue and applying a small sinusoidal voltage over a wide range of frequencies, the measured current response yields a characteristic electrical impedance spectrum of the tissue. Combining this characteristic electrical impedance spectrum with machine learning algorithms allows classification and identification of the tissue. EIS has been used to determine tissue types for different applications including oncology,[24] wound healing,[25] and biopsy.[26] Nevertheless, the use of EIS to characterize vascular occlusions is thus far limited to simple characterization of the electrical properties of in vitro thrombi.[27] In this article, we describe the combination of EIS with machine learning algorithms to create a novel and highly accurate method for the classification and identification of in vitro generated human thrombi.

METHODS
Thrombus analogs and sample categories
To demonstrate the applicability of EIS to the characterization of cerebral thrombi, we conducted a series of experiments on thrombi generated in vitro using citrated human blood from five healthy volunteers. Healthy donors were recruited under a protocol approved by the Toulouse Hospital

Bio-Resources biobank, declared to the French Ministry of Higher Education and Research (DC2016-2804). Blood was processed in accordance with hospital guidelines.

Five different protocols were used to generate three categories of thrombi based on RBC content and representative of thrombi commonly retrieved during EVT. Thrombi with low RBC content were prepared from platelet-poor plasma (PPP) or platelet-rich plasma (PRP) incubated at 37°C for 30 min in a Chandler loop at arterial blood flow levels, in the presence of 0.5 U/mL thrombin and 1 mM calcium chloride ($CaCl_2$) to trigger thrombus formation (thrombus types: 'PPP' and 'PRP', respectively). Thrombi with intermediate RBC content were generated using the same conditions of temperature, time, and blood flow, in the presence of 0.5 U/mL thrombin and 1 mM $CaCl_2$, but by incubating either equal volumes of isolated RBCs (prepared by centrifugation of whole blood at 190 g for 10 min) and PRP (thrombus type: '50RBC-50PRP'), or only whole blood (thrombus type: 'whole blood'). Thrombi with high RBC content were prepared by incubating whole blood under static conditions at 37°C for 60 min in the presence of 0.5 U/mL thrombin and 1 mM $CaCl_2$ to trigger RBC-rich thrombus formation (thrombus type: 'RBC static').

These five thrombus types were divided into three categories: 'White' RBC poor for PPP and PRP types, 'Red' for RBC static, 'Mixed' for 50RBC-50PRP and whole blood types. Two independent sets of thrombi were used: one to validate the composition of these three categories of thrombi by histological analysis (23 White, 18 Mixed, 12 Red thrombi), and the other to study their impedance signals (29 White, 26 Mixed, 12 Red thrombi). A fourth category labeled 'Blood' represents impedance measurements performed in liquid whole blood (n=67).

Histological analysis

Hematoxylin and eosin (H&E) staining was used on the first set of thrombi to identify the biological composition of representative thrombi from each category. Qupath software (Quantitative Pathology & Bioimage Analysis) was used to quantify RBC content. The mean values were calculated. Welch's t-test for equal means was also used on the five protocols (pairwise) to identify clusters of different RBC content. Significance level was α=0.01.

Impedance measurement and experimental design

Electrical impedance spectra of the second set of thrombi were acquired by sequentially applying a sinusoidal current excitation over the frequency range of 1 kHz to 30 MHz and measuring the associated impedance values.

A flexible custom-made microsensor made of polyimide and composed of a three-by-three electrode matrix was used (figure 1A), forming three rows of three electrodes. One impedance measurement was performed between two adjacent electrodes. For each microsensor a total of six measurements were performed between electrodes (two per array). In the following, one 'impedance measurement' refers to a measurement between two adjacent electrodes, while a 'complete acquisition' refers to the six measurements of the microsensor. The electrode size was 300×300 µm with an inter-electrode spacing of 450 µm. Each measurement between two electrodes probed an area of ∼1 mm×0.3 mm. The microsensor electrode arrays were rolled onto a rigid metal wire 300 µm in diameter and ∼2.5 cm long and fixed with glue. The three arrays were thus positioned around the wire, measuring the environment over its circumference using an E4990A Keysight impedance analyzer.

The experimental system is shown in figure 1B. The thrombus was placed in a plastic connector that immobilized the thrombus. This connector was part of a loop filled with heparinized blood (in static condition) to mimic the biological environment of a typical large-vessel occlusion. For the impedance analysis, the lower part of the microsensor with the electrodes was inserted either in blood or inside the thrombus, ensuring good contact between the electrodes and the sample (essential for the acquisition of a reliable measurement). Before each thrombus analysis, one complete impedance acquisition (six measurements) was made in liquid blood. Two or three complete acquisitions (6×2 or 6×3) were then performed with the electrodes contacting the thrombus at different locations to increase the diversity of measurements.

Liquid blood samples and the different thrombi were subdivided into five groups (one for each donor blood sample). For each group, three to four different microsensors were used to collect the impedance data.
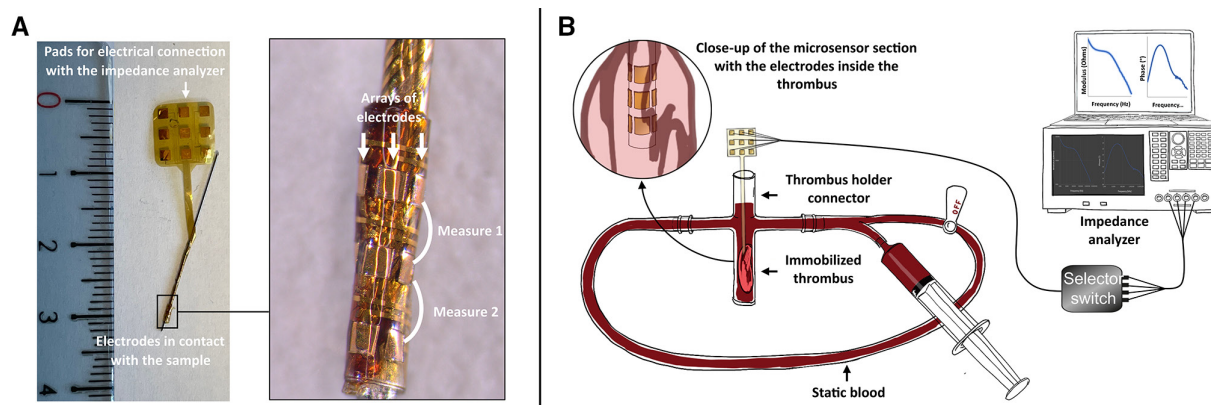

Figure 1 (A) Custom-made in vitro polyimide flexible device rolled over a 300 µm diameter metal wire (diameter comparable to a 0.014 inch neurovascular guidewire). The close-up shows the electrodes and indicates between which electrodes the measurement is performed. (B) Experimental setup. A custom-made microsensor was inserted in a thrombus holder filled with blood to mimic the environment of a large-vessel occlusion. For the measurement, the microsensor was inserted either in blood or in the thrombus while measurements were taken with the impedance analyzer. A custom-made selector switch allowed multiple measurements to be made on adjacent pairs of electrodes along each of the three rows of electrodes. Custom-made software is used to control the impedance analyzer.

Machine-learning approach

A support vector classifier (SVC) was first trained at the level of individual impedance measurements to predict one of four categories: Blood, White, Mixed, or Red. The labels of the individual measurements were defined according to the sample type (thrombus or liquid blood sample): the six individual measurements made in liquid blood with a given microsensor were all labeled with the category Blood, while the 12 (2×6) or 18 (3×6) individual measurements made in contact with a given thrombus of a category (White, Mixed, Red) were given their respective thrombus category label. The output of the SVC was the probability of an individual measurement to belong to a given category.

Predictions made on each individual measurement of a given sample were aggregated to build a single prediction by averaging the probabilities of each individual measurement to belong to each of the four categories (Blood, White, Mixed, and Red). The predicted category of a sample corresponded to the category with maximal averaged probability.

Evaluation of the performance by cross-validation

A cross-validation method was used to evaluate the predictive performance of the model, as is common when no dedicated test set is available. The overall prediction accuracy and, for each category, the sensitivity and specificity together with 95% confidence intervals (95% CI) were evaluated using the binomial distribution.[28]

A 'leave one group out' (LOGO) cross-validation scheme was chosen, where each group consisted of all the samples (blood and thrombi) from a given donor. To rule out bias in the validation set, a given sample should have all its individual measurements in either the training set or the validation set. Thus, five groups were chosen, one for each donor (to not have samples from the same donor in both the training and validation set). More specifically, the LOGO scheme corresponded to training the SVC on the dataset consisting of all samples from four donors, then evaluating the predictions on an isolated validation set of the fifth donor. The procedure was repeated by isolating another donor in the new validation set, and so on until predictions had been made for each single electrode pair measurements from all donors.

Data visualization with principal component analysis

The raw data were projected onto the first two principal components computed from the individual impedance measurement dataset.

Analysis pipeline

Scripts were written in Python 3.9. Machine-learning models, cross-validation scheme, and performance metrics were implemented using scikit-learn.[29]

RESULTS

Histological analysis

The first independent set of a total of 53 thrombi (23 White, 18 Mixed, 12 Red thrombi) were used to quantify their respective RBC content using H&E staining.

Figure 2A shows the RBC content of each sample by thrombus type. Among the five thrombus types, three clusters emerged with respect to their percentage of RBCs: White thrombi with nearly no RBCs obtained from the PPP and PRP; Mixed thrombi with intermediate values of RBC content obtained from either whole blood or 50RBC-50PRP; and Red thrombi with the highest values of RBC content obtained from RBC static thrombus type. Differences in the mean values for RBC content in between PPP and PRP as well as whole blood and 50RBC-50PRP were statistically non-significant, as shown by Welch's test for equal means at 0.01 significance level (comparison PPP/PRP: t statistic 1.83, p value 0.09; comparison whole blood/50RBC-50PRP: t statistic 2.32, p value 0.04). It justified grouping the PPP samples with the PRP samples, labeled White, and the whole
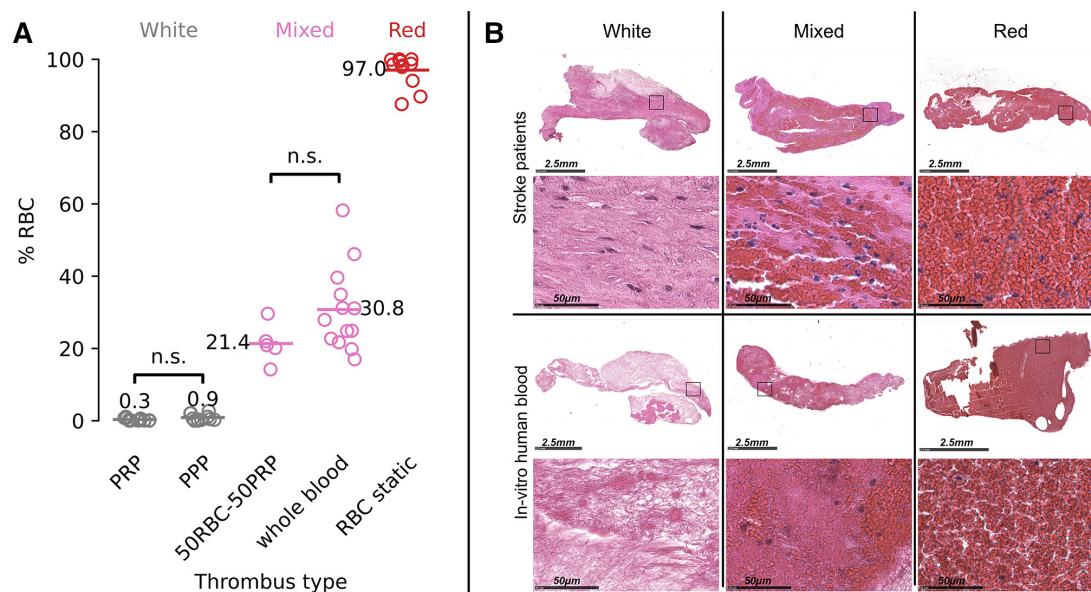

Figure 2 (A) Red blood cell (RBC) content by thrombus type. The mean values are represented by the lines, and the actual values are indicated by circles. From all pairwise Welch's t-tests of independence of the mean percentage of RBCs across thrombus types, only those non-significant (n.s.) at the 0.01 level are indicated for clarity. (B) Histological analysis of human thrombi retrieved by EVT (top) and in vitro generated thrombi using human blood (bottom). In the images, fibrin areas are pink, nucleated cells (eg, white blood cells) are blue, and RBCs are red. The black squares delineate the area where the zoom of the thrombus section is taken. EVT, endovascular thrombectomy; PPP, platelet-poor plasma; PRP platelet-rich plasma.

Table 1 Number of generated samples per category and per donor

Donor	Category	Samples	Spectra	Ratio (samples)	Ratio (spectra)
1	Blood	17	102	0.50	0.25
	Mixed	6	108	0.18	0.27
	Red	3	48	0.09	0.12
	White	8	144	0.24	0.36
2	Blood	12	72	0.5	0.25
	Mixed	5	90	0.21	0.31
	Red	2	36	0.08	0.12
	White	5	90	0.21	0.31
3	Blood	15	90	0.50	0.25
	Mixed	6	108	0.20	0.30
	Red	3	54	0.10	0.15
	White	6	108	0.20	0.30
4	Blood	13	78	0.50	0.25
	Mixed	5	90	0.19	0.29
	Red	2	42	0.08	0.13
	White	6	102	0.23	0.33
5	Blood	10	60	0.50	0.27
	Mixed	4	66	0.20	0.30
	Red	2	36	0.10	0.16
	White	4	60	0.20	0.27
All	Blood	67	402	0.50	0.25
	Mixed	26	462	0.19	0.29
	Red	12	216	0.09	0.14
	White	29	504	0.22	0.32

blood samples with the 50RBC-50PRP samples, labeled Mixed. All other pairwise comparisons showed significant differences in means (all p values <0.0011).

The thrombus fabrication methodology was also validated by comparing histological images obtained with H&E staining of the in vitro generated thrombi to those of real-world retrieved human thrombi. Figure 2B demonstrates that thrombi of the same category possess a comparable fibrin structure characterized by long intertwined fibers over the entire surface of the thrombus for White and Mixed thrombi, areas rich in RBCs for Mixed thrombi, and high RBC content for Red thrombi.

Prediction model
A total of 134 samples from the four defined categories were analyzed by impedance spectroscopy. Table 1 shows the content of the dataset for each donor of the cross-validation procedure. It includes the number of samples obtained for each donor, the number of spectra, and the ratio of the samples and spectra per category.

To assure a well-balanced LOGO cross validation, the ratios of individual measurements between categories were very similar across groups, with the exception of Red thrombi. Although the ratio of Blood samples was much larger than that of other categories, it was balanced at the individual spectrum level, since only one acquisition was performed for each liquid sample compared with the two/three acquisitions for each thrombus sample.

In contrast, the number of Red thrombi were systematically lower than in the other categories. This can be explained by

analyzing their impedance signature. Figure 3A,B shows a visualization of the two principal components of the impedance database for all the four categories and for three categories (White, Mixed, Blood), respectively. The principal component analysis (PCA) of figure 3A reveals that the impedance signal of Red thrombi was very clearly separated from the other thrombus categories, which in turn required collecting less data for this category. The differences between the other categories were less evident, as shown in the PCAs of figure 3A,B. However, by averaging the predictions on the level of the individual measurements of a sample to create one agglomerated prediction for the entire sample, higher prediction scores could be obtained. Figure 3C,D shows the prediction scores obtained per category with their 95% CI and the confusion matrix showing the prediction of the model against the histology for all the samples, respectively.

As shown in figure 3C,D, the global prediction accuracy was 88% with very high sensitivity and specificity for each category. Blood samples were predicted with very high specificity (99%) and sensitivity (90%), which translates to nearly perfect sensitivity of thrombus detection since specificity for the Blood category in figure 3C determines thrombus sensitivity and vice versa. The thrombi of the Red category were perfectly predicted with a specificity and sensitivity of 99% and 100%, respectively. A small number of blood samples were misidentified as Mixed thrombi, a few errors fell in the White/Mixed quadrant, and in very rare cases Mixed thrombi were mistakenly identified as Blood or Red thrombi. This can be explained by the high variability of the composition of Mixed thrombi, and measurements could thus have been taken in a thrombus area rich in either RBCs or in fibrin.

DISCUSSION AND CONCLUSIONS
This study describes a novel technique for characterizing thrombi occurring in acute ischemic stroke occlusions. The results demonstrate the ability of EIS, when combined with machine learning algorithms, to discriminate between blood and thrombi and to differentiate among Red, White, and Mixed thrombi with very high sensitivity and specificity. An obvious limitation of the present study is that the thrombi tested were generated in vitro using blood from healthy donors. We were, however, able to show that these thrombi are histologically very similar to those retrieved during EVT procedures. Ongoing research aims to create a predictive model for distinguishing human thrombus composition either ex vivo or directly in vivo. Efforts are also underway to increase the predictive performance of the technique, fine-tune the agglomeration techniques of the measurements, and improve signal quality.

A particularly exciting implication of the present work is that it raises the intriguing possibility of using this impedance-based technology during EVT to help identify an optimal patient-specific treatment strategy. The company Sensome has since developed a smart neurovascular guidewire integrating a proprietary miniaturized sensing technology to perform real-time impedance measurements (currently in clinical trial NCT04993079). The impedance sensor is integrated in the distal part of a 0.014 inch (356 μm) diameter neurovascular guidewire. Rather than having to select a thrombectomy device without information on thrombus composition, neurointerventionalists could potentially use such a smart guidewire to identify hard-to-retrieve thrombi, that is, platelet- and/or fibrin-rich thrombi, and choose a first-line treatment strategy that is specifically adapted to retrieve
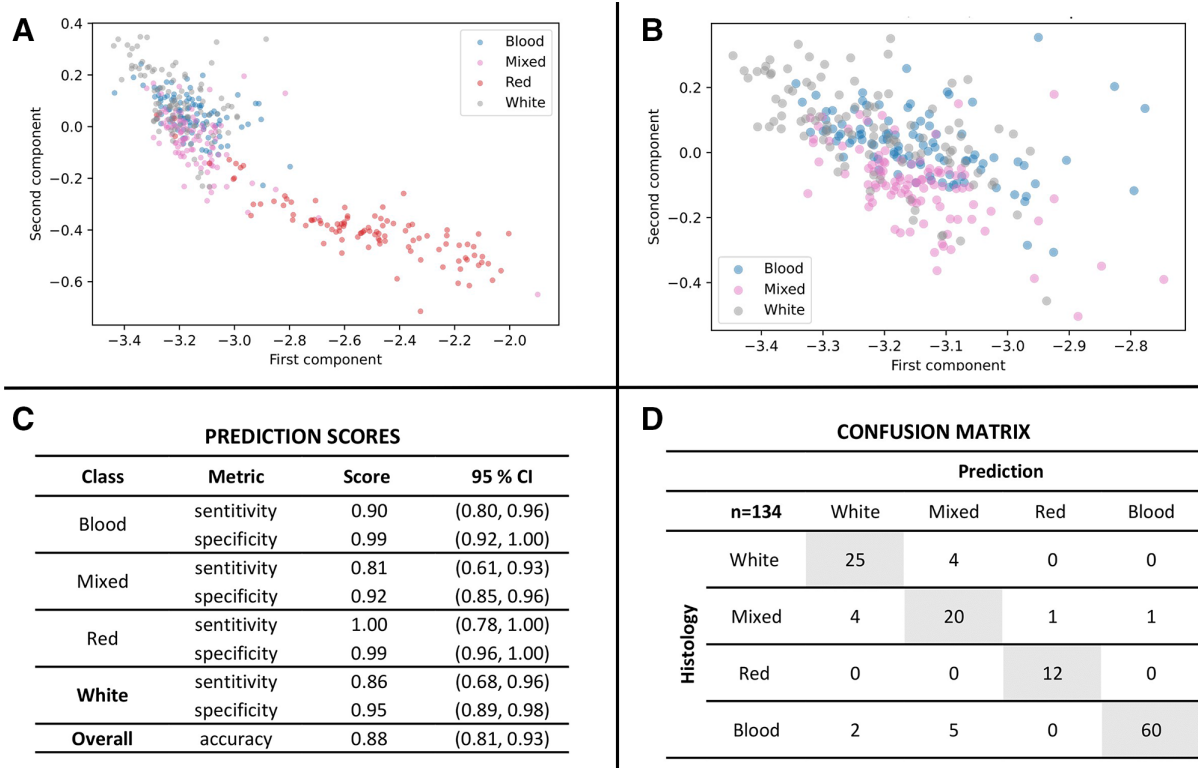
Figure 3 (A) Principal component analysis for the four categories (only 100 randomly selected impedance measurements per category are displayed to facilitate visualization). (B) Principal component analysis for the three categories excluding Red thrombi (only 100 randomly selected impedance measurements per category are displayed to facilitate visualization). (C) Human aggregate prediction scores with 95% confidence intervals (95% CI), and (D) the corresponding confusion matrix.

these types of thrombi. This promises, in turn, to increase the first-pass success of EVT with expected improved outcomes for patients.

ORCID iD
Pierluca Messina http://orcid.org/0000-0003-0624-9926

REFERENCES

1 Malhotra K, Gornbein J, Saver JL. Ischemic strokes due to large-vessel occlusions contribute disproportionately to stroke-related dependence and death: a review. *Front Neurol* 2017;8:651.
2 Zaidat OO, Castonguay AC, Linfante I, *et al*. First pass effect: a new measure for stroke thrombectomy devices. *Stroke* 2018;49:660–6.
3 Yoo AJ, Andersson T. Thrombectomy in acute ischemic stroke: challenges to procedural success. *J Stroke* 2017;19:121–30.
4 De Meyer SF, Andersson T, Baxter B, *et al*. Analyses of thrombi in acute ischemic stroke: a consensus statement on current knowledge and future directions. *Int J Stroke* 2017;12:606–14.
5 Merritt W, Holter AM, Beahm S, *et al*. Quantifying the mechanical and histological properties of thrombus analog made from human blood for the creation of synthetic thrombus for thrombectomy device testing. *J Neurointerv Surg* 2018;10:1168–73.
6 Lövblad K-O. Targeting the clot in acute stroke. *AJNR Am J Neuroradiol* 2018;39:E77.
7 Fitzgerald ST, Wang S, Dai D, *et al*. Platelet-rich clots as identified by Martius scarlet blue staining are isodense on NCCT. *J Neurointerv Surg* 2019;11:1145–9.

8 Staessens S, Fitzgerald S, Andersson T, *et al*. Histological stroke clot analysis after thrombectomy: technical aspects and recommendations. *Int J Stroke* 2020;15:467–76.

9 Douglas A, Fitzgerald S, Mereuta OM, *et al*. Platelet-rich emboli are associated with von Willebrand factor levels and have poorer revascularization outcomes. *J Neurointerv Surg* 2020;12:557–62.

10 Heo JH, Nam HS, Kim YD, *et al*. Pathophysiologic and therapeutic perspectives based on thrombus histology in stroke. *J Stroke* 2020;22:64–75.

11 Fitzgerald S, Rossi R, Mereuta OM, *et al*. Per-pass analysis of acute ischemic stroke clots: impact of stroke etiology on extracted clot area and histological composition. *J Neurointerv Surg* 2021;13:1111-1116.

12 Luthman AS, Bouchez L, Botta D, *et al*. Imaging clot characteristics in stroke and its possible implication on treatment. *Clin Neuroradiol* 2020;30:27–35.

13 Jolugbo P, Ariëns RAS. Thrombus composition and efficacy of thrombolysis and thrombectomy in acute ischemic stroke. *Stroke* 2021;52:1131–42.

14 Brinjikji W, Duffy S, Burrows A, *et al*. Correlation of imaging and histopathology of thrombi in acute ischemic stroke with etiology and outcome: a systematic review. *J Neurointerv Surg* 2017;9:529–34.

15 Maekawa K, Shibata M, Nakajima H, *et al*. Erythrocyte-rich thrombus is associated with reduced number of maneuvers and procedure time in patients with acute ischemic stroke undergoing mechanical thrombectomy. *Cerebrovasc Dis Extra* 2018;8:39–49.

16 Shin JW, Jeong HS, Kwon H-J, *et al*. High red blood cell composition in clots is associated with successful recanalization during intra-arterial thrombectomy. *PLoS One* 2018;13:e0197492.

17 Nikoubashman O, Dekeyzer S, Riabikin A, *et al*. True first-pass effect. *Stroke* 2019;50:2140–6.

18 Staessens S, Denorme F, Francois O, *et al*. Structural analysis of ischemic stroke thrombi: histological indications for therapy resistance. *Haematologica* 2020;105:498–507.

19 Bourcier R, Pautre R, Mirza M, *et al*. MRI quantitative T2* mapping to predict dominant composition of in vitro thrombus. *AJNR Am J Neuroradiol* 2019;40:59–64.

20 Darcourt J, Withayasuk P, Vukasinovic I, *et al*. Predictive value of susceptibility vessel sign for arterial recanalization and clinical improvement in ischemic stroke. *Stroke* 2019;50:512–5.

21 Bourcier R, Duchmann Z, Sgreccia A, *et al*. Diagnostic performances of the susceptibility vessel sign on MRI for the prediction of macroscopic thrombi features in acute ischemic stroke. *J Stroke Cerebrovasc Dis* 2020;29:105245.

22 Darcourt J, Garcia C, Phuong DM, *et al*. Absence of susceptibility vessel sign is associated with aspiration-resistant fibrin/platelet-rich thrombi. *Int J Stroke* 2021;16:972–80.

23 Patil S, Darcourt J, Messina P, *et al*. Characterising acute ischaemic stroke thrombi: insights from histology, imaging and emerging impedance-based technologies. *Stroke Vasc Neurol* 2022. doi:10.1136/svn-2021-001038. [Epub ahead of print: 03 Mar 2022].

24 Svoboda RM, Prado G, Mirsky RS, *et al*. Assessment of clinician accuracy for diagnosing melanoma on the basis of electrical impedance spectroscopy score plus morphology versus lesion morphology alone. *J Am Acad Dermatol* 2019;80:285–7.

25 Kekonen A, Bergelin M, Eriksson J-E, *et al*. Bioimpedance measurement based evaluation of wound healing. *Physiol Meas* 2017;38:1373–83.

26 Park J, Choi W-M, Kim K, *et al*. Biopsy needle integrated with electrical impedance sensing microelectrode array towards real-time needle guidance and tissue discrimination. *Sci Rep* 2018;8:264.

27 Santorelli A, Fitzgerald S, Douglas A. Dielectric profile of blood clots to inform ischemic stroke treatments*. In: *2020 42nd Annual International Conference of the IEEE Engineering in Medicine & Biology Society (EMBC)*, 2020.

28 Clopper CJ, Pearson ES. The use of confidence or fiducial limits illustrated in the case of the binomial. *Biometrika* 1934;26:404–13.

29 Pedregosa F, Varoquaux G, Gramfort A, *et al*. Scikit-learn: Machine Learning in Python. *Journal of Machine Learning Research* 2011;12:2825–30 https://jmlr.csail.mit.edu/papers/v12/pedregosa11a.html